Hybrid Materials

DOI: 10.1002/anie.201101383

Mesoscale Integration in Titania/J-Aggregate Hybrid Nanofibers**

Avinash J Patil, Young-Chul Lee, Ji-Won Yang, and Stephen Mann**

Self-assembly of molecular building blocks is a key strategy in the synthetic construction of multifunctional nanoscale architectures with unique characteristics.[1–3] Amongst a wide variety of possible supramolecular tectons, porphyrins and phthalocyanines are of special interest because of their inherent electronic and optical properties.[3–5] In particular, the programmed assembly of porphyrin molecules can produce quasi one-dimensional nanostructures (J-aggregates) that in part mimic complex supramolecular assemblies found in biology, such as the light harvesting center of green sulfur bacteria.[6,7] The spatial arrangement of molecular transition dipoles in these synthetic analogues facilitates strong coupling of the chromophores to produce higher-ordered nanostructures that could ultimately pave the way for fast excitation energy transfer over hundreds of molecules.[7] As a result, porphyrin-based nanostructures have been developed for use in photovoltaic devices,[2–5] and immobilized within organic/inorganic thin films or on virus particle surfaces for light-harvesting, energy-transport, photocatalysis, and sensing applications.[8–18]

Tetrakis(4-sulfonatophenyl)porphine (TPPS) is a water-soluble porphyrin that spontaneously self-assembles under aqueous acidic conditions to produce a range of supramolecular nanostructures.[19–24] In each case, the underlying structural motif is based on a "spread deck of cards" conformation or "staircase" arrangement of porphyrin monomers that gives rise to stacked supramolecular arrays with an average diameter of 1.7–2 nm, and which subsequently self-organize into higher-order J-aggregate superstructures to produce nanorods, nanotapes, or nanotubes with typical widths and lengths of 20–30 nm and several micrometers, respectively.[22,23] Significantly, recent studies have exploited anisotropic TPPS nanoparticles as template-directing agents to produce electrically conducting core–shell J-aggregate/polymer nanotubes,[25,26] metal nanowires,[27,28] optically responsive silica-coated J-aggregate nanotapes,[29] zinc-metalated nanotapes,[30] and J-aggregate nanotubes encased within ultrathin inorganic oxide layers of Al_2O_3 or TiO_2.[30] Whilst the above examples clearly highlight the versatility of integrating 20–30 nm-wide rods and tapes of TPPS into nanocomposite objects, transcription or encasement of the individual 1.7 nm-thick filaments of the primary J-aggregate stacked superstructure to produce functional hybrid nanomaterials with high spatial resolution remains unexplored. Herein, we describe a facile procedure for producing titania/J-aggregate nanorods and nanotapes that comprise an internally ordered hybrid mesostructure of co-aligned columnar arrays of $[H_4TPPS]^{2-}$ ions in which individual stacks of the porphyrin molecules are encased with oligomers of hydrolyzed/condensed titanium(IV) hydroxy/oxo species. We show that titania encapsulation of the porphyrin arrays at the molecular level preserves the optical and chiral properties and improves the hydrothermal stability of the J-aggregate supramolecular structure. We also demonstrate enhanced photocatalytic activity for the mesostructured hybrids compared to anatase nanoparticle dispersions of similar surface area, suggesting that close-to-molecular scale integration of the components has a significant influence on the rate of electron transfer and hole–electron pair recombination. Taken together, our results suggest that titania/J-aggregate mesostructured hybrids could have potential use in a wide range of applications involving optical and electronic processing, light harvesting, energy transport, sensing, or photocatalysis.

TEM images of unstained J-aggregate samples prepared by acidification of neutral solutions of $[H_2TPPS]^{4-}$ to produce $[H_4TPPS]^{2-}$ monomers at pH 2 showed the presence of a large number of flexible fiber- or tape-like structures that were uniform in width (20–30 nm) and variable in length (Supporting Information, Figure S1a). Hydrolysis of titanium diisopropoxide bis(acetylacetonate) (TDA) at pH 2 and room temperature in the presence of the preformed J-aggregate particles produced hybrid nanofibers that were typically 2–5 μm in length and 30–50 nm in width (Figure 1a). The increase in width was associated with a 10–20 nm-thick surface coating that was relatively smooth in texture. EDX analysis gave peaks for S and Ti corresponding to the presence of the sulfonated porphyrin and titania in the hybrid nanofibers, respectively, as well as Cl from the hydrochloric acid used during the acidification step (Figure 1a, inset). Surprisingly, high magnification TEM images of the hybrid nanofibers showed electron-dense fringes with a center-to-center distance of 3 nm ($\sigma = 0.26$ nm), and which ran parallel to the particle long axis (Figure 1b). The fringes remained unchanged across a tilt series of TEM images recorded from $-20°$ to $+20°$ (Supporting Information, Figure S2), indicating that the interior of the hybrid nanofibers consisted of an ordered 1D mesostructured array rather than

[*] Dr. A. J. Patil, Prof. S. Mann
Centre for Organized Matter Chemistry, School of Chemistry, University of Bristol
Bristol, BS8 1TS (UK)
E-mail: avinash.patil@bristol.ac.uk
s.mann@bristol.ac.uk
Y. C. Lee, Prof. J. W. Yang
Department of Chemical and Biomolecular Engineering (BK21), KAIST
Daejeon 305-701 (Republic of Korea)

[**] We thank the Global Frontier Program through Advanced Biomass R&D Centre (ABS) funded by the Ministry of Education, Science and Technology (MEST) and the University of Bristol for supporting this study.

Supporting information for this article is available on the WWW under http://dx.doi.org/10.1002/anie.201101383.

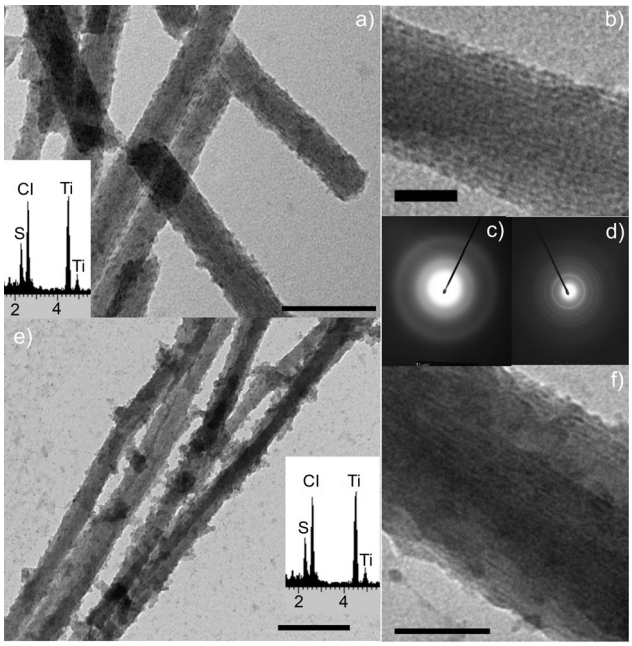

Figure 1. a) TEM image showing as-prepared titania/J-aggregate hybrid nanofibers. Scale bar = 100 nm. Inset: corresponding EDX analysis (keV units). b) High-resolution TEM image of an individual as-prepared titania/J-aggregate nanofiber showing periodic fringes running parallel to the long axis and corresponding to an internally ordered 1D mesostructure. Scale bar = 25 nm. c,d) Electron diffraction patterns for hybrid nanofibers before (c) and after hydrothermal aging at 75 °C for 6 h (d) showing presence of amorphous titania or anatase, respectively. e) Low-magnification TEM image of titania/J-aggregate nanofibers prepared by hydrothermal aging at 75 °C for 6 h and EDX analysis (inset, keV units). Scale bar = 200 nm. f) High-resolution TEM image of hydrothermally treated titania/J-aggregate nanofibers showing regularly spaced fringes corresponding to a mesostructured interior. Scale bar = 50 nm.

a lamellar arrangement of 2D sheets. This observation was consistent with the columnar packing of $[H_4TPPS]^{2-}$ anions into 1.7 nm-wide supramolecular stacks owing to orthogonal transition dipole interactions, and the subsequent bundling of these primary nanofilaments into mesostructured J-aggregate nanotubes/tapes.[22,23] Notably, no fringes were observed by high-resolution TEM analysis of the native J-aggregate nanofibers when viewed unstained or stained with uranyl acetate (Supporting Information, Figure S1b). This suggested that intercalation of polycationic species of hydrolyzed TDA between the porphyrin stacks was responsible for the high electron-density contrast, as well as the increase in *d* spacing from an expected value of 1.7 nm for the native mesostructure to 3 nm in the hybrid nanofibers. One possibility is that infiltration of hydrolyzed TDA into the J-aggregate nanofibers occurs by exchange with Na^+ ions that maintain electroneutrality between the columnar stacks of $[H_4TPPS]^{2-}$ anions.

Selective area electron diffraction and PXRD data indicated that amorphous titania was initially associated with the mesostructured J-aggregate nanofibers (Figure 1c), consistent with the presence of hydrolyzed TDA species and low levels of polycondensation. In contrast, similar studies on samples after hydrothermal treatment at 75 °C for up to 24 h showed a progressive transformation of the titania components into poorly ordered or nanocrystalline anatase (Figure 1d, Figure 2a). Corresponding TEM images showed an increase in the surface roughness and extent of aggregation of

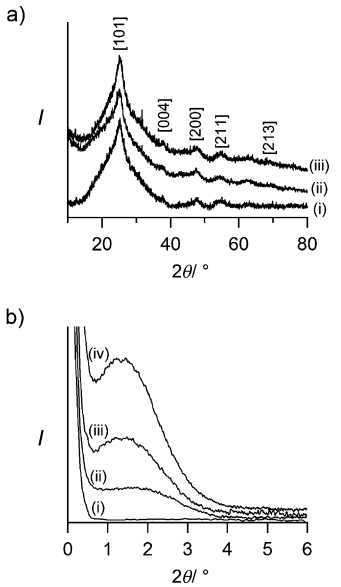

Figure 2. a) PXRD patterns of titania/J-aggregate mesostructured nanofibers after hydrothermal treatment at 75 °C for i) 6, ii) 12, and iii) 24 h. b) SAXS profiles of titania/J-aggregate nanofibres i) at room temperature and ii)–iv) after hydrothermal ageing at 75 °C for ii) 6, iii) 12, and iv) 24 h.

the titania-coated/impregnated nanofibers (Figure 1e). The increased surface roughness was associated with the presence of 4–7 nm-sized TiO_2 nanocrystallites that occasionally showed distinct lattice fringes often corresponding to the [101] plane ($d = 0.34$ nm) of anatase (data not shown). Furthermore, high-magnification images of the hydrothermally aged samples displayed well-defined fringes running parallel to the morphological long axis with a spacing of 4.4 nm ($\sigma = 0.56$ nm; Figure 1f) that was independent of the tilt angle (Supporting Information, Figure S3) The results indicated that the titania/J-aggregate stacked mesostructure present within the interior of the hybrid nanofibers was retained after hydrothermal treatment. Moreover, hydrothermally induced polycondensation of TDA species within the interstitial spaces of the J-aggregate columnar array would account for the 1.4 nm increase in lattice spacing compared with the as-prepared hybrid materials. This was consistent with SAXS profiles that showed a single broad low-angle band that progressively increased in intensity and *d* spacing as the hydrothermal ageing time was increased (Figure 2b). For example, samples aged for 6 or 24 h showed a 1D mesostructure spacing of about 5 or 6 nm, respectively. Although anatase crystallization was clearly associated with the surface of the hybrid nanofibers, we could not rule out the possibility that this phase was also formed within the internal mesostructure; however, given the confined dimensions, it seems more likely that amorphous titania resides within the inter-columnar interstices.

Supramolecular packing of $[H_4TPPS]^{2-}$ ions within the titania/J-aggregate mesostructured nanofibers was investigated using UV/Vis and circular dichroism (CD) spectroscopy. UV/Vis spectra of the nanocomposites before or after hydrothermal treatment exhibited a Soret band at 434 nm and three Q bands at 490, 646, and 709 nm that were virtually unchanged from the native J-aggregate nanofibers (Figure 3a).[29] The band intensities were progressively decreased

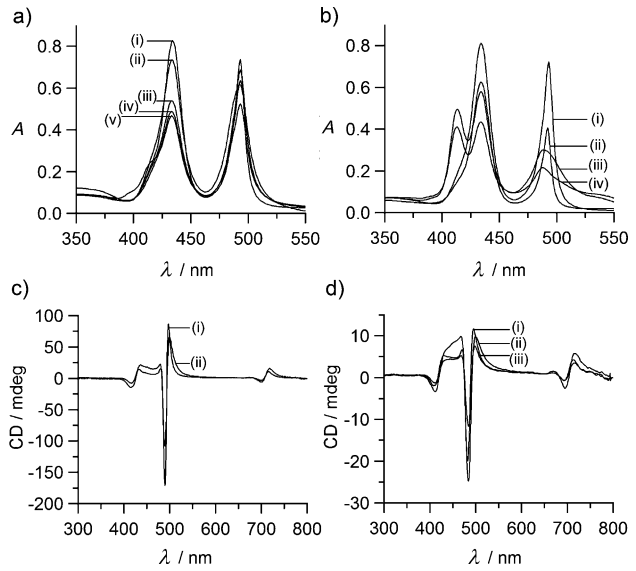

Figure 3. a) UV/Vis absorption spectra of i) native and ii)–v) titania/J-aggregate mesostructured nanofibers showing changes in the Soret (434 nm) and Q band (490 nm) intensities: ii) titania/J-aggregate nanofibers at room temperature and iii)–v) after hydrothermal ageing at 75 °C for iii) 6, iv) 12, and v) 24 h. b) UV/Vis spectra of i) native J-aggregate nanofibers at room temperature and ii)–iv) after hydrothermal treatment at 75 °C for ii) 6, iii) 12, and iv) 24 h; appearance of a new band at 413 nm is associated with partial disassembly and formation of porphyrin monomers. c) CD spectra of i) native J-aggregate nanofibers and ii) titania/J-aggregate mesostructured nanofibers at room temperature. d) Titania/J-aggregate mesostructured nanofibers hybrids after hydrothermal treatment at 75 °C for i) 6, ii) 12, and iii) 24 h. CD bands are observed at about 490, 497, and 712 nm. Negative and positive features at about 418 and 434 nm are attributed to Soret band absorptions.

with increasing hydrothermal ageing time, which was attributed to increasing levels of aggregation of the $[H_4TPPS]^{2-}$ building blocks, as confirmed by hydrothermal treatment of the native J-aggregate solutions (Figure 3b). Moreover, extended hydrothermal reaction times between 12 and 24 h gave rise to an additional absorbance at 413 nm in the native J-aggregate nanotapes owing to partial disassembly of the stacked supramolecular structure and formation of free $[H_2TPPS]^{4-}$ monomer units (Figure 3b). In contrast, no monomers were observed in the titania/J-aggregate hybrid nanostructures (Figure 3a), confirming that encapsulation of the porphyrin arrays increased the thermal stability of the supramolecular assemblies.

CD spectra of the native J-aggregate nanotapes at room temperature showed a strongly split Cotton effect with intense negative and positive signals at 490 nm, and 497 and 712 nm, respectively. (Figure 3c).[19] Similar spectra were recorded for the mesostructured titania/J-aggregate nanofibers prepared at room temperature although the band intensities were reduced and slightly red-shifted (Figure 3c), suggesting that the mesoscopic chiral structure of the J-aggregates was only marginally affected by complexation with the TDA precursor. CD spectra of hydrothermally aged native J-aggregate nanotapes showed ill-defined and red-shifted positive signals at 503 and 722 nm, or 520, 735, and 738 nm after 6 or 12 h, respectively, indicating significant deterioration in superstructural chirality (Supporting Information, Figure S4). In contrast, the hydrothermally treated mesostructured titania/J-aggregate nanofibers maintained their chiral integrity, displaying the characteristic negative signal at 490 nm along with slight shifts in the positive bands (500, 720 nm; 503, 720 nm; 506, 722 nm at 6, 12, and 24 h, respectively; Figure 3d). These results were in good agreement with the UV/Vis spectroscopy data and collectively indicated that encasement of the porphyrin chromophores within the ultrathin inorganic matrix of the nanohybrid construct not only preserved the optical and chiral properties of the $[H_4TPPS]^{2-}$ supramolecular aggregates but also improved their tolerance with respect to prolonged hydrothermal treatment.

Brunauer–Emmett–Teller (BET) isotherms using N_2 desorption gave a surface area of 42 $m^2 g^{-1}$ for the mesostructured titania/J-aggregate nanofibers prepared at room temperature, which increased to values of 188, 211, and 170 $m^2 g^{-1}$ for samples hydrothermally treated for 6, 12, or 24 h, respectively. The increased surface area observed after 12 h compared with 6 h was consistent with transformation of the surface coating of amorphous titania into anatase nanoparticles, whilst the reduced value obtained after 24 h was associated with increased levels of particle aggregation for more prolonged periods of hydrothermal processing. Similar surface area values were determined for anatase nanoparticles prepared under identical conditions but in absence of the J-aggregate nanotapes (236, 250, or 224 $m^2 g^{-1}$ after 6, 12, or 24 h, respectively). We therefore tested the UV-induced photocatalytic activity of the mesostructured nanofibers by investigating the kinetics of oxidative degradation of a common organic pollutant (phenol) at pH 6.8. Time dependent log concentration plots confirmed that the kinetics of phenol photodegradation followed first-order behavior in agreement with the Langmuir–Hinshelwood model (Figure 4). Moreover, the photocatalytic activity of the titania/J-aggregate nanohybrids was increased at all hydrothermal times compared with the corresponding samples of anatase nanoparticles prepared in the absence of the porphyrin nanotapes (Figure 4). The initial rates were 0.0480, 0.0662, and 0.0350 h^{-1} for mesostructured titania/J-aggregate nanofibers aged at 75 °C for 6, 12, and 24 h, respectively, compared with 0.0226 h^{-1} (6 h), 0.021 h^{-1} (12 h), and 0.0105 h^{-1} (24 h) for the control sample of anatase nanoparticles. Thus, in both series of samples the rate of photodegradation with respect to the hydrothermal processing time was $12 > 6 > 24$ h, which is consistent with the surface-area values. However, although the control anatase samples had higher surface areas, and were therefore expected to show better catalytic perfor-

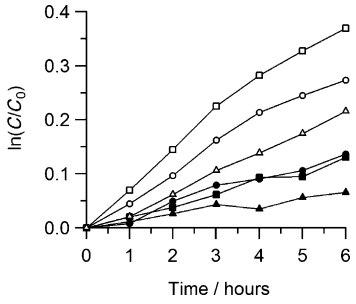

Figure 4. Plots of $\ln(C_o/C)$ versus time (C_o = initial concentration of phenol, C = concentration of phenol at t) showing relative rates of UV-mediated photocatalytic degradation of phenol in the presence of control samples of anatase nanoparticles hydrothermally prepared at 75 °C for 6 (●), 12 (■), or 24 h (▲) or in the presence of titania/J-aggregate nanofibers hydrothermally aged at 6 (○), 12 (□), or 24 (△) h.

mance, the observed lower photocatalytic response suggested increased recombination of the photogenerated electron–hole pairs in the absence of the J-aggregate phase.[31] Correspondingly, the higher catalytic activity observed for hybrid nanofibers may originate from facilitated electron transfer and reduced hole–electron pair recombination arising from electronic interactions at the titania–porphyrin interface within the mesostructured material.[14]

The above results suggest that the formation of meso-ordered titania/J-aggregate superstructures can be attributed to weak electrostatic interactions between the primary arrays of stacked $[H_4TPPS]^{2-}$ anions and polycationic titanium (IV) hydroxyl/oxo species produced by hydrolysis and condensation of TDA in acidic solutions.[32] Use of TDA was critical to the formation of the integrated mesostructure; indeed, no internal periodicity was observed when titanium isopropoxide (TIP) was used as a precursor (Supporting Information, Figure S5). Compared with TIP, the rates of hydrolysis and condensation of TDA are highly controlled by the slow release of the acetylacetonate chelating ligand such that bulk precipitation is markedly inhibited.[33] As a consequence, infiltration of hydrolyzed TDA polycations into the J-aggregate stacked superstructure is competitive with binding and accumulation of these species at the surface of the porphyrin nanofibers. Thus, by appropriate design of the reaction conditions each 1.7 nm-wide columnar array of porphyrin molecules can be wrapped in a 0.6–2.2 nm-thick sheath of hydrolyzed/condensed titanium(IV) oligomers/polymers, and the individual nanorods or nanotapes of the hybrid mesostructure coated with an ultrathin external shell of titania. As a result, the encased J-aggregate supramolecular structure exhibits unmodified optical and chiral properties, is stabilized against prolonged hydrothermal ageing, and shows enhanced photocatalytic activity. We envisage that similar facile methods of controlled mesoscale integration in hybrid nanofibers could be readily extended to other porphyrin/phthalocyanine supramolecular structures provided that they comprise exchangeable counterions or can be readily swollen by solvents to facilitate host–titania interactions. Such materials should have potential applications as novel hybrid components in electronic and optical devices, energy capture and transport systems, as well as in chemical sensing and reactivity.

Experimental Section

Tetrakis(4-sulfonatophenyl)porphine J-aggregates were prepared by acidifying of an aqueous solution of TPPS (50 μM, 10 mL) using hydrochloric acid (1 M). Acidification resulted in an immediate pink to bright-green color change owing to protonation of $[H_2TPPS]^{4-}$ ions and formation of the diacid $[H_4TPPS]^{2-}$ monomer. The acidified solution (pH ≈ 1.98) was stirred overnight and then used as described below.

Preparation of titania/J-aggregate mesostructures was undertaken as follows. Typically, a stock solution of titanium diisopropoxide bis(acetylacetonate) (0.02058 M in isopropanol, 10 μL) was added to a dispersion of J-aggregate nanorods (50 μM, 500 μL), and the mixture was stirred overnight. The green-colored dispersion was then characterized as described below, or hydrothermally treated by transfer to a Teflon-lined stainless steel reactor and aged at 75 °C for 6, 12, and 24 h. A similar procedure was also undertaken using titanium (IV) isopropoxide.

For catalytic experiments, as-prepared and hydrothermally aged titania/J-aggregate dispersions or control samples of anatase nanoparticles were isolated by ultracentrifugation. A sample of the sediment (20 mg) was then dispersed in phenol solution (5 mg L^{-1}, 40 mL) and equilibrated for 30 min in the dark. The reaction mixtures were then irradiated using a UV lamp (365 nm, UVP model UVLS-26 EL Series 6 W, 115 V–60 Hz). Photocatalytic degradation of phenol was monitored by withdrawing aliquots at regular time intervals, and the change in absorbance and degradation monitored by UV/Vis spectroscopy and high-performance liquid chromatography (HPLC, Waters, USA; methanol/water 50:45 v/v, flow rate 1 mL min^{-1}, 214 nm detector range), respectively.

TEM images were taken of air-dried samples using a JEOL 1200 EX microscope operating at 120 kV or JEOL JEM 2100 instrument with EDX analysis (Oxford Instruments, ISIS300). PXRD patterns and small-angle X-ray scattering (SAXS) were assessed using D/MAX-RB (Rigaku, 12 kW) and D/MAX-2500 (Rigaku) instrumentation, respectively. N_2 sorption/desorption data were obtained using a gas sorption analyzer (NOVA 4200 Ver. 7.10), and the specific surface area values were calculated by using the BET equation. UV/Vis and circular dichroism spectra were recorded at room temperature using a Perkin-Elmer Lambda 25 spectrophotomer and JASCO J-810 spectrometer (quartz cell, path length = 10 mm and 1 mm), respectively.

Received: February 24, 2011
Published online: December 7, 2011

Keywords: hybrid materials · J-aggregates · photocatalysis · self-assembly

[1] L. C. Palmer, S. I. Stupp, *Acc. Chem. Res.* **2008**, *41*, 1674 – 1684.
[2] F. J. M. Hoeben, P. Jonkheijm, E. W. Meijer, A. P. H. J. Schenning, *Chem. Rev.* **2005**, *105*, 1491 – 1546.
[3] M. S. Choi, T. Yamazaki, I. Yamazaki, T. Aida, *Angew. Chem.* **2004**, *116*, 152 – 160; *Angew. Chem. Int. Ed.* **2004**, *43*, 150 – 158.
[4] G. D. Scholes, G. Rumbles, *Nat. Mater.* **2006**, *5*, 683 – 696.
[5] D. M. Eisele, J. Knoester, S. Kirstein, J. P. Rabe, D. A. Vanden Bout, *Nat. Nanotechnol.* **2009**, *4*, 658 – 663.
[6] V. I. Prokhorenko, D. B. Steensgaard, A. R. Holzwarth, *Biophys. J.* **2003**, *85*, 3173 – 3186.
[7] J. M. Olson, *Photochem. Photobiol.* **1998**, *67*, 61 – 75.
[8] T. Ogi, S. Ito, *Thin Solid films* **2006**, *500*, 289 – 295.

[9] E. I. Mal'tsev, D. A. Lypenko, B. I. Shapiro, M. A. Brusentseva, G. H. W. Milburn, J. Wright, A. Hendriksen, V. I. Berendyanev, B. V. Kotov, A. V. Vannikov, *Appl. Phys. Lett.* **1999**, *75*, 1896 – 1898.
[10] A. S. R. Koti, N. Periasamy, *Chem. Mater.* **2003**, *15*, 369 – 371.
[11] G. De Luca, G. Pollicino, A. Romeo, L. M. Scolaro, *Chem. Mater.* **2006**, *18*, 2005 – 2007.
[12] W. Xu, H. Guo, D. L. Akins, *J. Phys. Chem. B* **2001**, *105*, 1543 – 1546.
[13] K. Lang, P. Bezdicka, J. Bourdelande, J. Hernando, I. Jirka, E. Kafunkova, F. Kovanda, P. Kubat, J. Mosinger, D. M. Wagnerova, *Chem. Mater.* **2007**, *19*, 3822 – 3829.
[14] Y. Fujii, Y. Tsukahara, Y. Wada, *Bull. Chem. Soc. Jpn.* **2006**, *79*, 561 – 568.
[15] A. D. Schwab, D. E. Smith, B. Bond-Watts, D. E. Johnston, J. Hone, A. T. Johnson, J. C. de Paula, W. F. Smith, *Nano Lett.* **2004**, *4*, 1261 – 1265.
[16] H. Tokuhisa, P. Hammond, *Adv. Funct. Mater.* **2003**, *13*, 831 – 839.
[17] A. L. Yeats, A. D. Schwab, B. Massare, D. E. Johnston, A. T. Johnson, J. C. de Paula, W. F. Smith, *J. Phys. Chem. C* **2008**, *112*, 2170 – 2176.
[18] Y. S. Nam, T. Shin, H. Park, A. P. Magyar, K. Choi, G. Fantner, K. A. Nelson, A. M. Belcher, *J. Am. Chem. Soc.* **2010**, *132*, 1462 – 1463.
[19] J. M. Ribo, J. Crusats, F. Sagues, J. Claret, R. Rubires, *Science* **2001**, *292*, 2063 – 2066.
[20] A. D. Schwab, D. E. Smith, C. S. Rich, E. R. Young, W. F. Smith, J. C. de Paula, *J. Phys. Chem. B* **2003**, *107*, 11339 – 11345.
[21] R. Rotomskis, R. Augulis, V. Snitka, R. Valiokas, B. Liedberg, *J. Phys. Chem. B* **2004**, *108*, 2833 – 2838.
[22] Y. Kitahama, Y. Kimura, K. Takazawa, *Langmuir* **2006**, *22*, 7600 – 7604.
[23] V. Snitka, M. Rackaitis, R. Rodaite, *Sens. Actuators B* **2005**, *109*, 159 – 166.
[24] C. Escudero, J. Crusats, I. Diez-Perez, Z. El-Hachemi, J. M. Ribo, *Angew. Chem.* **2006**, *118*, 8200 – 8203; *Angew. Chem. Int. Ed.* **2006**, *45*, 8032 – 8035.
[25] T. Hatano, M. Takeuchi, A. Ikeda, S. Shinkai, *Chem. Lett.* **2003**, *32*, 314 – 315.
[26] T. Hatano, A.-H. Bae, M. Takeuchi, A. Ikeda, S. Shinkai, *Bull. Chem. Soc. Jpn.* **2004**, *77*, 1951 – 1957.
[27] Z. Wang, C. J. Medforth, J. A. Shelnutt, *J. Am. Chem. Soc.* **2004**, *126*, 15954 – 15955.
[28] Z. Wang, C. J. Medforth, J. A. Shelnutt, *J. Am. Chem. Soc.* **2004**, *126*, 16720 – 16721.
[29] P. J. Meadows, E. Dujardin, S. R. Hall, S. Mann, *Chem. Commun.* **2005**, 3688 – 3690.
[30] L. Zhang, A. J. Patil, L. Li, A. Schierhorn, S. Mann, U. Gosele, M. Knez, *Angew. Chem.* **2009**, *121*, 5082 – 5085; *Angew. Chem. Int. Ed.* **2009**, *48*, 4982 – 4982.
[31] A. L. Linsebigler, G. Lu, J. T. Yates, *Chem. Rev.* **1995**, *95*, 735 – 758.
[32] H. Wang, A. J. Patil, K. Liu, S. Petrov, S. Mann, M. A. Winnik, I. Manners, *Adv. Mater.* **2009**, *21*, 1805 – 1808.
[33] U. Schubert, N. Husing, A. Lorenz, *Chem. Mater.* **1995**, *7*, 2010 – 2027.

